

Enforcing causality in nonrelativistic equations of state at finite temperature

Constantinos Constantinou^{1,*} and Madappa Prakash^{2,†}

¹*Institute for Advanced Simulation, Institut für Kernphysik, and Jülich Center for Hadron Physics, Forschungszentrum Jülich, D-52425 Jülich, Germany*

²*Department of Physics and Astronomy, Ohio University, Athens, OH 45701*
(Dated: December 5, 2021)

We present a thermodynamically consistent method by which equations of state based on nonrelativistic potential models can be modified so that they respect causality at high densities, both at zero and finite temperature (entropy). We illustrate the application of the method using the high density phase parametrization of the well known APR model in its pure neutron matter configuration as an example. We also show that, for models with only contact interactions, the adiabatic speed of sound is independent of the temperature in the limit of very large temperature. This feature is approximately valid for models with finite-range interactions as well, insofar as the temperature dependence they introduce to the Landau effective mass is weak. In addition, our study reveals that in first principle nonrelativistic models of hot and dense matter, contributions from higher than two-body interactions must be screened at high density to preserve causality.

Keywords: Hot and dense matter, nonrelativistic potential models, speed of sound.

PACS numbers: 21.65.Mn, 26.50.+x, 51.30.+i, 97.60.Bw

I. INTRODUCTION

The precise determination of neutron star masses close to $2M_\odot$ [1, 2], prospects of observing gravitational waves (GW's) from mergers involving binary neutron stars as in the recent detection of GW's from mergers of binary black holes [3, 4], and the hope of observing a nearby core-collapse supernova (SN) with the several neutrino observatories currently in place have greatly strengthened the study of dense matter physics. Central to this study is the equation of state (EOS) of dense matter at both zero and finite temperature. Depending on the values of the baryon densities, n , and temperatures, T , reached in core-collapse supernovae, neutron stars from their birth to old age, and mergers of compact binary stars, several phases of matter may be encountered. At high densities and/or temperatures, these phases may consist of strangeness-bearing hadrons and/or quark matter [5].

Large-scale computer simulations of the astrophysical phenomena mentioned above employing the microscopic physics input of model EOS's from both nonrelativistic and relativistic approaches have indicated the ranges of n/n_s , where $n_s \simeq 0.16 \text{ fm}^{-3}$ is the nuclear saturation density, T , and the net electron fraction $Y_e = n_e/n$ encountered. To enable simulations, EOS's that range over n/n_s up to 10, T up to 200 MeV, and Y_e up to 0.6 are required. These conditions imply an entropy per baryon S (in units of Boltzmann's constant k_B) of up to 200. In varying amounts the entropy is shared between the hadrons, leptons, and photons. For EOS's with only nucleonic components, S_{nuc} of up to 4-5 is not uncommon.

In the homogeneous phase ($n \geq 0.1 \text{ fm}^{-3}$) and using the EOS of APR [6], $S \leq 30$ with nucleons contributing about 5, leptons 15, and photons 10. The highest density at which $S \sim 200$ is about 0.01 fm^{-3} (at $T=200$ MeV) with 95% of the contributions coming from leptons and photons. The dependence of these numbers on the charge/lepton fraction is, generally, very weak.

The focus of this paper is on the adiabatic speed of sound c_s in matter at high density and temperature. In hydrodynamical simulations, c_s represents a physical scale which controls the macroscopic evolution of matter. Thus, a quantitative knowledge of how c_s varies with n and T (or S) in models of hot, dense matter can shed light on the time development of involved hydrodynamical simulations. In physical systems, c_s cannot exceed the speed of light c . Nevertheless, many of the EOS's used to describe nucleonic matter have nonrelativistic underpinnings and therefore do not conform to the requirement of causality. (Relativistic field-theoretical approaches to dense matter inherently respect causality, and will not be addressed further in this work.) For some nonrelativistic EOS's, typically the softer ones, which struggle to support neutron star (NS) masses $\sim 2M_\odot$, the causality requirement is only violated for densities beyond their scope. The stiffer EOSs however, can become problematic for densities and temperatures for which hadronic matter is expected to persist within a star.

Repulsive contributions to the energy per particle $E(u = n/n_s)$ that vary faster than linear in u give rise to acausal behavior at high densities. Thus, higher than two-body forces found necessary to achieve saturation at the empirical n_s with the empirical binding energy of symmetric nuclear matter (SNM) must screen themselves with progressively increasing density to ensure causal behavior. Following the suggestion in Ref. [7], causality was maintained through the use of $Bu^\sigma/(1 + B'u^{\sigma-1})$,

* c.constantinou@fz-juelich.de

† prakash@ohio.edu

where B is a constant of dimension energy and B' is a dimensionless constant appropriately chosen to have c_s approach c from below, in the explorative study of Ref. [8]. This implied self-screening of repulsive interactions, while desirable, is not always guaranteed in nonrelativistic potential-model calculations. This issue is particularly relevant to modern microscopic calculations of the EOS of SNM and pure neutron matter (PNM), such as the quantum Monte Carlo [9–11] and chiral effective field theory approaches [12–19] in which the role of three-body forces at $T = 0$ have been examined. Owing to inherent technical difficulties, calculations have been limited up to about $2n_s$ in both of these approaches. To calculate the structural properties of NS's, the EOS's have been extrapolated beyond $\sim 2n_s$ through the use of piece-wise polytropes that respect causality (thus screening the influence of 3-body forces present at $n < 2n_s$, possibly prematurely for higher densities). This polytropic extrapolation, while satisfactory at $T = 0$ on a practical level, cannot however be extended to finite temperature unless the effects of temperature on the EOS are known a priori.

Here, we present a thermodynamically consistent method to maintain causality for EOS's that become acausal at both zero and finite temperature. While such a method is available in the literature for zero temperature [6, 20, 21], a method to encompass the influence of temperature on c_s has not received much attention (the method presented in Appendix E of our earlier work in Ref. [6] contained an inadvertent error, which is corrected in this work). We illustrate the application of the method using a few chosen models [22–24] that become acausal at high density and temperature. These models have distinctly different behaviors in their nucleon effective masses as functions of density. For simplicity, results for PNM are shown in all cases with the generalization to a multi-component system indicated in the text. We stress, however, that the applicability of the method proposed is not limited to the class of models chosen for illustration. As long as the relevant thermodynamic variables such as the energy, pressure, and chemical potential for any model are available for all densities and temperatures of interest, the method can be used to render the EOS causal and to satisfy the thermodynamic identity.

The paper is organized as follows. In Sec. II, the adiabatic speed of sound c_s is defined in terms of thermodynamic quantities characteristic of an EOS at both zero and finite temperature. This section also contains a discussion of the behavior of c_s in the limiting cases of degenerate and nondegenerate bulk matter. The method devised to implement causality for EOS's that become acausal at high densities and temperatures is described in Sec. III. In Sec. IV, the numerical procedure to enforce causality for models with contact interactions is detailed. Results in the case of PNM for these models are presented in Sec. V both at zero and finite temperature. Additionally, results for a model in which contributions from higher than two-body interactions are screened to

prevent an acausal behavior are presented. Section VI presents a summary and conclusions.

II. GENERAL CONSIDERATIONS

For small-amplitude perturbations, the velocity v of fluid particles obeys the wave equation [25]

$$\frac{\partial^2 v}{\partial t^2} - c_s^2 \frac{\partial^2 v}{\partial x^2} = 0 \quad (1)$$

whose solution $f(x - c_s t)$ represents longitudinal sound wave propagation with speed c_s under the condition of adiabatic motion for which $\partial S / \partial t = 0$, where S is the entropy. Thus small density fluctuations in a compressible fluid propagate at the speed of sound given by [26–28]

$$\left(\frac{c_s}{c}\right)^2 = \frac{\partial P}{\partial \epsilon} \Big|_S = \frac{\partial P / \partial n \Big|_S}{\partial \epsilon / \partial n \Big|_S} \quad (2)$$

$$= \frac{1}{\mu + m} \frac{\partial P}{\partial n} \Big|_S = \frac{K_S}{9(\mu + m)} = \frac{\Gamma_S P}{h + mn}, \quad (3)$$

where P is the pressure, ϵ is the energy density, n is the number density, $h = nE + P$ is the specific enthalpy density, μ is the chemical potential, $K_S = 9 \partial P / \partial n \Big|_S$ the adiabatic incompressibility, and $\Gamma_S = \partial \ln P / \partial \ln n \Big|_S$ the adiabatic index. In the variables (n, T) , we can also express c_s as [27, 29]

$$\left(\frac{c_s}{c}\right)^2 = \frac{C_P}{C_V} \frac{n}{h + mn} \frac{\partial P}{\partial n} \Big|_T, \quad (4)$$

where C_P and C_V are the specific heats at constant pressure and volume, respectively.

We will begin our analysis with nonrelativistic models that are described by the generic Hamiltonian density

$$\mathcal{H} = \frac{\hbar^2}{2} \frac{\tau(n, S)}{m^*(n)} + V(n), \quad (5)$$

where the first term is the kinetic energy density and the second is the potential energy density. The quantity m^* is the Landau effective mass defined at the Fermi surface by $m^*(n) = p_F (\partial \epsilon_p / \partial p) \Big|_{p_F}$, where ϵ_p is the single particle spectrum and p_F is the Fermi momentum. Models that employ contact interactions such as Skyrme models, the APR model, and other microscopic models that employ the effective mass approximation as indicated above are examples of the representation in Eq. (5). As our discussion proceeds, we will consider other cases, *e.g.*, models in which finite-range interactions at various levels of sophistication are considered and in which additional complications are encountered. Some physical insight is gained by examining the behavior of c_s in the limiting situations of degenerate and nondegenerate bulk matter to which we turn below.

Degenerate case

For conditions such that $T/T_F \ll 1$ (or, equivalently $S \leq 1$), where $T_F = p_F^2/(2m^*)$ is the Fermi temperature in nonrelativistic models, degenerate conditions prevail. In this case, the leading-order Fermi liquid theory (FLT) expressions for the thermal components of the pressure and energy density are given by [30, 31]

$$P_{th}(n, T) = \frac{2}{3}naT^2Q \quad \text{and} \quad \epsilon_{th}(n, T) = naT^2 \quad (6)$$

$$\text{with} \quad Q = 1 - \frac{3}{2} \frac{n}{m^*} \frac{dm^*}{dn}, \quad (7)$$

where $a = \pi^2/(4T_F)$ is the level density parameter. Utilizing the leading-order FLT result $S = 2aT$, we get

$$P_{th}(n, S) = \frac{S^2}{6} \frac{nQ}{a} = \frac{2S^2}{3\pi^2} nT_FQ \quad \text{and} \quad (8)$$

$$\epsilon_{th}(n, S) = \frac{S^2}{4} \frac{n}{a} = \frac{S^2}{\pi^2} nT_F, \quad (9)$$

from which the density derivatives at constant S

$$\begin{aligned} \left. \frac{dP_{th}}{dn} \right|_S &= \frac{P_{th}}{n} \left(1 + \frac{2}{3}Q + \frac{n}{Q} \frac{dQ}{dn} \right), \\ \left. \frac{d\epsilon_{th}}{dn} \right|_S &= \frac{\epsilon_{th}}{n} \left(1 + \frac{2}{3}Q \right) \quad \text{and}, \\ \left. \frac{dT}{dn} \right|_S &= \frac{2}{3} \frac{TQ}{n}, \end{aligned} \quad (10)$$

are easily obtained. Putting together the other components in the total P and ϵ , we arrive at

$$\begin{aligned} \left. \frac{dP}{dn} \right|_S &= \frac{2}{5}T_F \left(1 + \frac{2}{3}Q \right) + n \frac{d^2V}{dn^2} + \left. \frac{dP_{th}}{dn} \right|_S \\ \left. \frac{d\epsilon}{dn} \right|_S &= m + \frac{3}{5}T_F \left(1 + \frac{2}{3}Q \right) + \frac{dV}{dn} + \left. \frac{d\epsilon_{th}}{dn} \right|_S, \end{aligned} \quad (11)$$

where the first term in the first equation above and the second term in the second represent the $T = 0$ results of the kinetic parts. These results allow us to appreciate how c_s^2 is governed by physical quantities in special circumstances.

(i) The case when $V = 0$: When the thermal contributions can be regarded as small ($S \leq 1$) compared to their zero temperature counterparts,

$$c_s^2 \simeq \frac{2}{5} \frac{T_F}{m} \left(1 + \frac{2}{3}Q \right) \quad (12)$$

$$= \frac{1}{5} \left(\frac{p_F}{m^*} \right)^2 \frac{m^*}{m} \left(1 + \frac{2}{3}Q \right). \quad (13)$$

The physical scale of c_s here is the velocity at the Fermi surface $v_F = p_F/m^*$ modified by m^*/m and its logarithmic derivative with respect to density contained in Q . For $m^*(n) = m$, the ideal gas value of $c_s^2 = (1/3)(p_F/m)^2$ is recovered from Eq. (13).

(ii) Density-dependent $V(n)$: In order to achieve equilibrium at the empirical nuclear density $n_0 \simeq 0.16 \text{ fm}^{-3}$ with the empirical energy per particle of $\simeq -16 \text{ MeV}$, and to support the precisely determined neutron star masses of $2M_\odot$'s, models of dense nuclear matter have employed contributions from beyond 2-body forces in $V(n)$ that vary as $n^{2+\epsilon}$. If these contributions persist at densities $n \gg n_0$, and dominate over the other contributions including the thermal parts ($S \leq 1$), causality is bound to be violated. Consider, for example, $V(n) \propto n^\sigma$ for which

$$\left(\frac{c_s}{c} \right)^2 \simeq \frac{n}{dV/dn} \frac{d^2V/dn^2}{dV/dn} = \sigma - 1, \quad (14)$$

which for $\sigma \geq 2$ renders $(c_s/c)^2 \geq 1$.

(iii) Additional contributions to the density-dependent $V(n)$: As apparent from Eq. (11), both the $S = 0$ and $S \neq 0$ terms contribute in determining the magnitude of $(c_s/c)^2$. The interplay between these terms is also determined by $m^*(n)$ and its density derivatives as well as by $Q(n)$ and its derivatives. In Skyrme-like models in which $m^*/m = (1 + \beta n)^{-1}$ with β a constant, the kinetic energy density, $\epsilon_{kin} \propto n^{5/3}(1 + \beta n)$, so that at some high n the $n^{8/3}$ term dominates causing the EOS to become acausal. In some cases, acausality can set in at lower densities for $S \neq 0$ than for $S = 0$. A quantitative discussion of results from models with different behaviors of m^*/m vs n will be deferred to Sec. V.

Nondegenerate case

At zero temperature (entropy), c_s is a function of just the density n . As we show below, the same is true for nonrelativistic models with only contact interactions in the limit of very large entropy/temperature, *i.e.*, the extreme nondegenerate limit. Here, the entropy is given by the Sackur-Tetrode relation

$$S = \frac{5}{2} - \ln \left[\left(\frac{2\pi\hbar^2}{m^*T} \right)^{3/2} \frac{n}{2} \right], \quad (15)$$

where m^* is the density-dependent Landau effective mass. Solving Eq. (15) for the temperature, we get

$$T = \frac{2\pi\hbar^2}{m^*} \left(\frac{n}{2} \right)^{2/3} \exp \left(\frac{2}{3}S - \frac{5}{3} \right), \quad \left. \frac{\partial T}{\partial n} \right|_S = \frac{2}{3} \frac{TQ}{n}, \quad (16)$$

with Q given by Eq. (7). In this case, thermal effects dominate over cold matter contributions (exclusive of rest-mass) to thermodynamic properties. Consequently,

$$\left(\frac{c_s}{c} \right)^2 \xrightarrow{S \gg 1} \frac{\partial P_{th}/\partial n|_S}{m + \partial \epsilon_{th}/\partial n|_S}. \quad (17)$$

For nonrelativistic contact-interaction models in the non-degenerate limit,

$$P_{th} = nTQ, \quad \left. \frac{\partial P_{th}}{\partial n} \right|_S = TQ \left(1 + \frac{2}{3}Q + \frac{n}{Q} \frac{dQ}{dn} \right) \quad (18)$$

$$\varepsilon_{th} = \frac{3}{2}nT, \quad \left. \frac{\partial \varepsilon_{th}}{\partial n} \right|_S = \frac{3}{2}T \left(1 + \frac{2}{3}Q \right). \quad (19)$$

When the mass term dominates over the thermal part in the denominator of Eq. (17), and $Q \simeq 1$ as is the case when the effects of interactions are small,

$$\left(\frac{c_s}{c} \right)^2 \xrightarrow{S \gg 1} \frac{5}{3} \frac{T}{m} \quad (20)$$

which is the result for one-component classical gases. The physical scale of c_s here is the thermal velocity of particles. In the case that the thermal component of the denominator in Eq. (17) dominates over the mass,

$$\left(\frac{c_s}{c} \right)^2 \xrightarrow{S \gg 1} \frac{2}{3} \frac{Q \left(1 + \frac{2}{3}Q + \frac{n}{Q} \frac{dQ}{dn} \right)}{1 + \frac{2}{3}Q}, \quad (21)$$

that is, the temperature/entropy dependence drops out with the result $(c_s/c)^2 \simeq 2/3$ for $Q \simeq 1$. It must be emphasized that this result is obtained only at very high temperatures for which the use of nonrelativistic considerations becomes questionable.

Models with finite-range forces

Finite-range forces introduce momentum dependences (other than p^2) to the single-particle potential which in turn cause it to acquire a temperature dependence [29]. The effects of these interactions can still be collected in a density- and temperature-dependent function $m^*(n, T)$ which, however, can no longer be identified with the Landau effective mass. Nevertheless, if this T -dependence is weak, then

$$m^*(n, T) \simeq m^*(n, 0) + T \left. \frac{\partial m^*(n, T)}{\partial T} \right|_{T=0} + \dots \quad (22)$$

$$\equiv m^*(1 + bT) \quad (23)$$

where $m^* = m^*(n, 0)$ is the Landau mass and $b(n) \equiv (1/m^*) \partial m^*(n, T)/\partial T|_{T=0}$ such that $bT \ll 1$. Combining Eq. (15) with $m^* \rightarrow m^*(n, T)$ and Eq. (23), and expanding in a Taylor series for $bT \ll 1$, we find

$$S \simeq \frac{5}{2} - \ln \left[\left(\frac{2\pi\hbar^2}{m^*T} \right)^{3/2} \frac{n}{2} \right] + \frac{3bT}{2}. \quad (24)$$

Perturbative inversion of Eq. (24) yields, in the second recursion,

$$T \simeq \frac{2\pi\hbar^2}{m^*} \left(\frac{n}{2} \right)^{2/3} \exp \left[\frac{2}{3}S - \frac{5}{3} - \frac{2\pi\hbar^2}{m^*} b \left(\frac{n}{2} \right)^{2/3} \exp \left(\frac{2}{3}S - \frac{5}{3} \right) \right]. \quad (25)$$

We now substitute $2\pi\hbar^2(n/2)^{2/3} \exp(2S/3 - 5/3)$ by $m^*(n, T)$, then replace $m^*(n, T)$ by $m^*(1 + bT)$ to get

$$T \simeq \frac{2\pi\hbar^2}{m^*} \left(\frac{n}{2} \right)^{2/3} \exp \left[\frac{2}{3}S - \frac{5}{3} - \frac{bTm^*(n, T)}{m^*} \right] \\ \simeq \frac{2\pi\hbar^2}{m^*} \left(\frac{n}{2} \right)^{2/3} \exp \left[\frac{2}{3}S - \frac{5}{3} - bT(1 + bT) \right]. \quad (26)$$

Now dropping b^2T^2 and expanding the exponential for small bT ,

$$T \xrightarrow{\frac{bT \ll 1}{S \gg 1}} \frac{2\pi\hbar^2}{m^*} \left(\frac{n}{2} \right)^{2/3} \exp \left(\frac{2}{3}S - \frac{5}{3} \right). \quad (27)$$

This result shows that in the extreme nondegenerate limit, finite-range force models with weak T -dependence in their m^* 's will behave similarly to zero-range models and thus they will also obey Eq. (21).

III. IMPLEMENTATION OF CAUSALITY

The general approach described below is more conveniently applied in the variables (n, S) that are natural to the speed of sound as opposed to (n, T) commonly used in tabulations of EOS properties. Working with the former set allows us to carry out all calculations analytically circumventing the need for numerical integration.

Causality is preserved as long as the speed of sound c_s is less than or equal to the speed of light c :

$$\left(\frac{c_s}{c} \right)^2 \equiv \beta = \frac{\partial P}{\partial \epsilon} \Big|_S = \frac{\partial P}{\partial n} \Big|_S \left(\frac{\partial \epsilon}{\partial n} \Big|_S \right)^{-1} \leq 1. \quad (28)$$

Here the total energy density ϵ is inclusive of the internal energy density ε and the rest-mass energy density mn :

$$\epsilon = \varepsilon + mn. \quad (29)$$

By making use of

$$P = n^2 \frac{\partial(\epsilon/n)}{\partial n} \Big|_{S, N} = n \frac{\partial \epsilon}{\partial n} \Big|_{S, N} - \varepsilon \quad (30)$$

and

$$\frac{\partial P}{\partial n} \Big|_{S, N} = n \frac{\partial^2 \varepsilon}{\partial n^2} \Big|_{S, N} \quad (31)$$

where N is the number of nucleons in the system, we write Eq. (28) as a second-order differential equation (DE)

$$\frac{\partial^2 \varepsilon}{\partial n^2} \Big|_{S, N} - \frac{\beta}{n} \frac{\partial \varepsilon}{\partial n} \Big|_{S, N} = \frac{\beta m}{n}. \quad (32)$$

Thus, in addition to entropy conservation, in our approach we must impose the condition of baryon number conservation and, in the case of multicomponent systems,

fixed composition. Equation (32), can be reduced to a first-order DE

$$\left. \frac{\partial \xi}{\partial n} \right|_{S,N} - \frac{\beta}{n} \xi = \frac{\beta m}{n} \quad (33)$$

by setting

$$\xi = \left. \frac{\partial \varepsilon}{\partial n} \right|_{S,N} = \mu + TS. \quad (34)$$

Note that the combination of Eqs. (30) and (34) yields the thermodynamic identity $\varepsilon + P = n\mu + Ts$. The solution of Eq. (33) requires that β is mapped to some function $\beta_f(n, S) \leq 1 \forall (n, S)$. This implies that the causality-fixing density n_f obtained from

$$\beta(n, S) - \beta_f(n, S) = 0 \quad (35)$$

is an entropy-dependent function.

The approach of c_s to c depends on the choice of $\beta_f(n, S)$. For our illustrative calculations below, some choices of $\beta_f(n, S)$ are considered.

Density-independent $\beta_f(n, S)$

For such a constant β_f , the integrating factor corresponding to Eq. (33) is given by

$$f(n) = \exp\left(-\beta_f \int \frac{dn}{n}\right) = n^{-\beta_f}, \quad (36)$$

and has the property

$$\frac{d}{dn}[n^{-\beta_f} \xi] = n^{-\beta_f} \frac{\beta_f m}{n}. \quad (37)$$

Integration of Eq. (37) leads to

$$\xi = \left. \frac{\partial \varepsilon}{\partial n} \right|_{S,N} = -m + c_1 n^{\beta_f}, \quad (38)$$

where c_1 is a constant of integration. A second integration results in

$$\varepsilon = -mn + \frac{c_1 n^{\beta_f+1}}{\beta_f+1} + c_2 \quad (39)$$

with another constant of integration c_2 , and therefore

$$P = c_1 \frac{\beta_f}{\beta_f+1} n^{\beta_f+1} - c_2. \quad (40)$$

The constants c_1 and c_2 are determined by the boundary conditions

$$\varepsilon[n_f(S), S] = \varepsilon_f(S) \quad (41)$$

$$P[n_f(S), S] = P_f(S), \quad (42)$$

where n_f is the causality fixing density, defined by Eq. (35). The functional forms of $\varepsilon(n, S)$ and $P(n, S)$ are those obtained from the original Hamiltonian density.

From Eqs. (41) and (42), we get

$$c_1 = \frac{\varepsilon_f + mn_f + P_f}{n_a^{\beta_f+1}} \quad (43)$$

$$c_2 = \frac{1}{\beta_f+1} [\beta_f(\varepsilon_f + mn_f) - P_f]. \quad (44)$$

Thus the energy density and the pressure are given by

$$\varepsilon = -mn + \frac{(\varepsilon_f + mn_f + P_f)}{\beta_f+1} \left(\frac{n}{n_f}\right)^{\beta_f+1} + \frac{\beta_f(\varepsilon_f + mn_f) - P_f}{\beta_f+1} \quad (45)$$

$$P = \frac{\beta_f}{\beta_f+1} (\varepsilon_f + mn_f + P_f) \left(\frac{n}{n_f}\right)^{\beta_f+1} - \frac{\beta_f(\varepsilon_f + mn_f) - P_f}{\beta_f+1}. \quad (46)$$

The chemical potential μ is straightforwardly obtained from $\mu = \xi - TS$. Equations (45) and (46) can be used for $n \geq n_f$ with a fixed $\beta_f \leq 1$ so that causality is never violated and such that the thermodynamic identity is obeyed thus ensuring thermodynamic consistency. At this stage, we must reiterate the point that ε and P as given in Eqs. (45) and (46) are functions of (n, S) . The switch to (n, T) is easily achieved by setting

$$\varepsilon(n, T) = \varepsilon[n, S(n, T)] \quad (47)$$

$$P(n, T) = P[n, S(n, T)] \quad (48)$$

$$\beta(n, T) = \beta[n, S(n, T)]. \quad (49)$$

Note that the procedure outlined above for $T \neq 0$ closely mirrors that for $T = 0$ described in Appendix E of our earlier work in Ref. [6], but with the use of appropriate quantities at finite T . The method outlined in Ref. [6] for $T \neq 0$ was flawed in that Eq. (E18) there defining the chemical potential lacked a term involving TS , that is, μ was taken to be $\partial\varepsilon/\partial n|_{S,N}$ instead of the correct $\partial\varepsilon/\partial n|_{S,V}$ where $n = N/V$. Equation (34) in this work corrects that error. Moreover, the assumption that $C_P/C_V = \text{constant}$ was made, which is only true in the degenerate limit ($S \leq 1$) where $C_P/C_V \simeq 1$.

Density-dependent $\beta_f(n, S)$

We emphasize that β_f need not be a constant. Consider, for the purposes of illustration, the function

$$\beta_f(n, S) = a_1 + \frac{a_2 n^{a_3}}{1 + a_4 n^{a_3}} \quad (50)$$

where the a_i are real numbers; a_1 and a_3 are unitless while a_2 and a_4 have units fm^{3a_3} . For this β_f to approach 1 from below they must all be positive and $a_1 + a_2/a_4 = 1$; $a_1 > 0$ also ensures that Eq. (35) always has a solution. Moreover, if the fraction $a_2/(a_3 a_4)$ is an integer, then ξ , ε , and P are relatively simple functions of the density.

For example, if we choose $a_1 = 1/2$, $a_2 = 2$, $a_3 = 1$, and $a_4 = 4$ then

$$\beta_f = \frac{1}{2} + \frac{2n}{1+4n} \quad (51)$$

$$\xi = -m + c_1 n^{1/2} (1+4n)^{1/2} \quad (52)$$

$$\varepsilon = -mn + \frac{c_1}{16} \left[n^{1/2} (1+4n)^{1/2} (1+8n) - \frac{1}{2} \sinh^{-1}(2n^{1/2}) \right] + c_2 \quad (53)$$

$$P = -\frac{c_1}{16} \left[n^{1/2} (1+4n)^{1/2} (1-8n) - \frac{1}{2} \sinh^{-1}(2n^{1/2}) \right] - c_2. \quad (54)$$

For the choice $a_1 = 4/5$, $a_2 = 2$, $a_3 = 1/5$, and $a_4 = 10$, we get

$$\beta_f = \frac{4}{5} + \frac{2n^{1/5}}{1+10n^{1/5}} \quad (55)$$

$$\xi = -m + c_1 (n^{4/5} + 10n) \quad (56)$$

$$\varepsilon = -mn + \frac{5}{9} c_1 (n^{9/5} + 9n^2) + c_2 \quad (57)$$

$$P = c_1 \left(\frac{4}{9} n^{9/5} + 5n^2 \right) - c_2. \quad (58)$$

Of course, many other possibilities exist for the a_i above, as well as for the generic functional form of β_f .

IV. NUMERICAL NOTES

Here we describe the procedure to calculate $(c_s/c)^2$ for the Hamiltonian density in Eq. (5) for conditions of arbitrary degeneracy. The analytical results obtained in Sec. II for the degenerate and nondegenerate cases serve as a check for the results obtained in this section. To calculate the finite-entropy properties corresponding to Eq. (5), we employ the Johns, Ellis and Lattimer (JEL) [32] scheme in which the Fermi-Dirac integrals

$$F_\alpha = \int_0^\infty \frac{x^\alpha}{e^{x-\psi} + 1} dx \quad (59)$$

are expressed as algebraic functions of a single parameter f related to the entropy via

$$S = \frac{5}{3} \frac{F_{3/2}(f)}{F_{1/2}(f)} - \psi(f) \quad (60)$$

where [6]

$$F_{3/2}(f) = \frac{3f(1+f)^{1/4-M}}{2\sqrt{2}} \sum_{m=0}^M p_m f^m \quad (61)$$

$$F_{1/2}(f) = \frac{f(1+f)^{1/4-M}}{\sqrt{2(1+f/a)}} \sum_{m=0}^M p_m f^m \times \left[1+m - \left(M - \frac{1}{4} \right) \frac{f}{1+f} \right] \quad (62)$$

$$\psi(f) = \frac{\mu(n, S) - V(n)}{T(n, S)} = 2(1+f/a)^{1/2} + \ln \left[\frac{(1+f/a)^{1/2} - 1}{(1+f/a)^{1/2} + 1} \right] \quad (63)$$

The values of the coefficients appearing in Eqs. (61)-(63) are $a = 0.433$, $M = 3$, $p_0 = 5.34689$, $p_1 = 16.8441$, $p_2 = 17.4708$, and $p_3 = 6.07364$. We note that the F_α are connected via their derivatives with respect to ψ according to $\partial F_\alpha / \partial \psi = \alpha F_{(\alpha-1)}$. The JEL scheme enables a rapid and an accurate evaluation of the thermodynamic quantities preserving thermodynamic consistency.

The kinetic energy density τ and the number density n are related to $F_{3/2}$ and $F_{1/2}$, respectively:

$$\tau(n, S) = \frac{\gamma}{2\pi^2} \left[\frac{2m^*(n)T(n, S)}{\hbar^2} \right]^{5/2} F_{3/2}[f(S)] \quad (64)$$

$$n = \frac{\gamma}{2\pi^2} \left[\frac{2m^*(n)T(n, S)}{\hbar^2} \right]^{3/2} F_{1/2}[f(S)], \quad (65)$$

where $\gamma = 1(2)$ for PNM(SNM) and $f(S)$ is the solution of Eq. (60). From Eq. (65), it follows that

$$T(n, S) = \left(\frac{\pi^2 \hbar^3}{\gamma \sqrt{2}} \right)^{2/3} \frac{n^{2/3}}{m^*(n)} \frac{1}{F_{1/2}^{2/3}[f(S)]} \quad (66)$$

and

$$\left. \frac{\partial T(n, S)}{\partial n} \right|_S = \frac{2Q(n)}{3n} T(n, S) \quad (67)$$

with $Q(n)$ given by Eq. (7). The total energy density is given by

$$\epsilon(n, S) = \mathcal{H}(n, S) + mn \quad (68)$$

and thus

$$\left. \frac{\partial \epsilon}{\partial n} \right|_S = \frac{5}{3n} \frac{\hbar^2}{2} \frac{\tau(n, S)}{m^*(n)} \left[1 - \frac{3n}{5m^*} \frac{dm^*}{dn} \right] + \frac{dV}{dn} + m. \quad (69)$$

The pressure is obtained from

$$P(n, S) = n \left. \frac{\partial \epsilon}{\partial n} \right|_S - \epsilon(n, S) \quad (70)$$

$$= \frac{2}{3} \frac{\hbar^2}{2} \frac{Q(n)}{m^*(n)} \tau(n, S) + n \frac{dV}{dn} - V(n) \quad (71)$$

and therefore

$$\frac{\partial P}{\partial n}\Big|_S = n \frac{d^2 V}{dn^2} + \frac{10}{9} \frac{\hbar^2}{2} \frac{Q(n)}{m^*(n)} \tau(n, S) \times \left[1 - \frac{3n}{5m^*(n)} \frac{dm^*}{dn} + \frac{3n}{5Q(n)} \frac{dQ}{dn} \right]. \quad (72)$$

In the causality-fixing regime [$n \geq n_f(S)$], Eqs. (45) and (46) imply

$$\frac{\partial \epsilon}{\partial n}\Big|_S = \frac{\partial \epsilon}{\partial n}\Big|_S + m = \frac{(\epsilon_f + mn_f + P_f)}{n_f} \left(\frac{n}{n_f} \right)^{\beta_f} \quad (73)$$

$$\frac{\partial P}{\partial n}\Big|_S = \frac{\beta_f}{n_f} (\epsilon_f + mn_f + P_f) \left(\frac{n}{n_f} \right)^{\beta_f}. \quad (74)$$

Correspondingly, $(c_s/c)^2 = \beta_f$ as indicated earlier.

For the conversion of ϵ , P , and c_s to the (n, T) variables, we must first express the entropy in terms of n and T . This is accomplished by solving

$$n = \frac{\gamma}{2\pi^2} \left[\frac{2m^*(n)T}{\hbar^2} \right]^{3/2} F_{1/2}(f) \quad (75)$$

for $f(n, T)$ which is then used as input in the functions that appear in Eq. (60).

V. RESULTS

In this section, we present results pertaining to the speed of sound for the PNM models of APR [6, 24], LS [22], and SLy4 [23] and the alterations our causality-enforcing scheme causes to the properties of the neutron stars in their maximum-mass configurations. This configuration reaches the largest central density and therefore it is the setting where the effects of causality implementation will be most apparent. Our results also illustrate how various thermodynamic functions are modified by this approach in the case of PNM for the EOS of APR.

Figure 1 shows the squared speed of sound of the three models for PNM for different values of the entropy. Results for APR and LS are qualitatively similar in that for densities lower than a certain density n_X , the higher-entropy curves lie higher whereas the situation is reversed for densities $n > n_X$. Consequently, causality for finite entropies (temperatures) is violated at densities that are higher than those at zero temperature for these two models. The intersection point at intermediate densities is common to all curves (for each model) and thus independent of the entropy. Its value is obtained by solving

$$\left(\frac{c_s}{c} \right)_{S=0}^2 - \left(\frac{c_s}{c} \right)_{S \gg 1}^2 = 0, \quad (76)$$

where the first term refers to the squared speed of sound in cold matter and the second term is given by Eq. (21).

The speed of sound of SLy4 on the other hand, is a monotonically increasing function of the entropy and hence the causality-violating density n_a decreases with

increasing entropy. The n_a for the three models at $S=0$, 3, and 5 as well as the fixed points n_X of APR and LS are given in Table I.

Property	APR	LS	SLy4
$n_{a,0}(\text{fm}^{-3})$	0.870(0.841)	1.112(1.092)	1.181(1.298)
$n_{a,3}(\text{fm}^{-3})$	0.914(0.849)	1.232(1.165)	0.608(0.814)
$n_{a,5}(\text{fm}^{-3})$	2.710(0.994)	1.774(1.478)	0.307(0.454)
$n_X(\text{fm}^{-3})$	0.809(0.830)	0.671(0.708)	N/A

TABLE I. Densities at which causality is violated at $S=0$, 3, and 5 for APR, LS, and SLy4 in their PNM(SNM) configuration and intersection density (where applicable).

The differences in the results of c_s^2 for the three models are related to the behaviors of the effective masses and their derivatives with respect to density as reflected in the function $Q(n)$ and its derivative with respect to density. Figure 2 shows results of m^*/m and $Q(n)$ vs density. For the LS model here, $Q(n) = 1$ as $m^*(n) = m$, the vacuum nucleon mass. For the APR and SLy4 models, m^*/m decreases monotonically with density, the variation in the latter case being substantially more than for the former. These variations are in turn reflected in the behaviors of $Q(n)$ with n for these two models. These results clearly indicate the crucial role of the density dependence of the effective mass on the speed of sound in hot, dense matter.

Tables II-IV list the maximum mass and the corresponding radius and central number density n_c , total energy density ϵ_c , and pressure P_c for different values of β_f at $T = 0$. The last column in each table displays these quantities as obtained using the original causality-violating EOS. As β_f is increased toward 1, M_{max} , n_c , ϵ_c , and P_c approach their pre-implementation values from below whereas R_{max} does so from above. Changes to these quantities (compared to pre-implementation) are small; about 10% even for $\beta_f = 0.5$, with the notable exception of the central pressure P_c which nearly halves. For LS, the $\beta_f = 0.9$ star is identical to the original because $n_f(\beta_f = 0.9)$ exceeds the central density of the star. A similar consideration applies for SLy4 for which $n_f(\beta_f = 0.9)$ is relatively close to n_c .

β_f	0.5	0.7	0.9	Not Fixed
Prop.				
$n_f(\text{fm}^{-3})$	0.547	0.667	0.796	N/A
$M_{max}(M_\odot)$	2.00	2.13	2.18	2.20
$R_{max}(\text{km})$	10.61	10.46	10.31	10.16
$n_c(\text{fm}^{-3})$	1.107	1.096	1.101	1.111
$\epsilon_c(\text{MeV fm}^{-3})$	1398.6	1433.3	1472.0	1507.0
$P_c(\text{MeV fm}^{-3})$	516.0	691.9	851.1	1005.1

TABLE II. PNM neutron star properties for the APR model for different values of β_f at $T = 0$.

Figure 3 shows how the squared speed of sound of APR (PNM) is altered by our method as a function of the density for fixed entropy (left panel) and for fixed tempera-

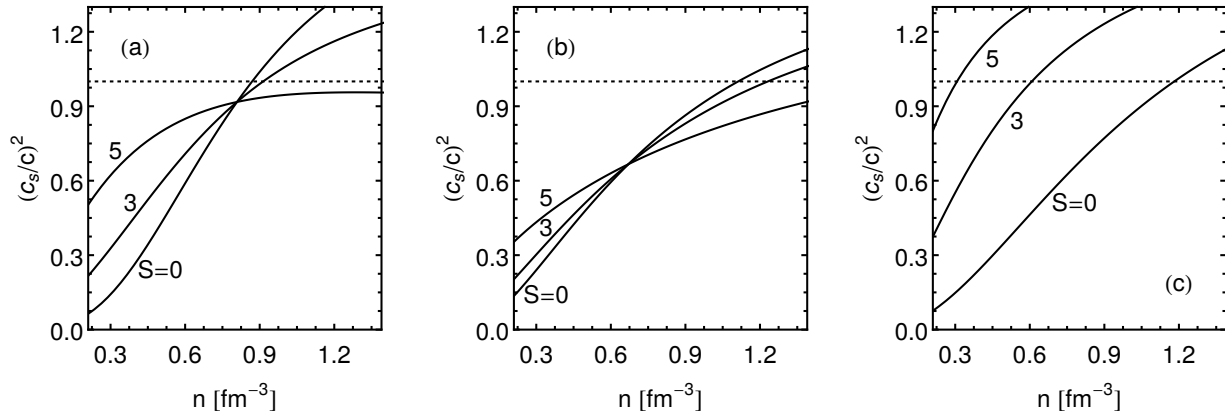


FIG. 1. Squared speed of sound vs density in PNM for the models of APR (a), LS (b), and SLy4 (c) at fixed entropy.

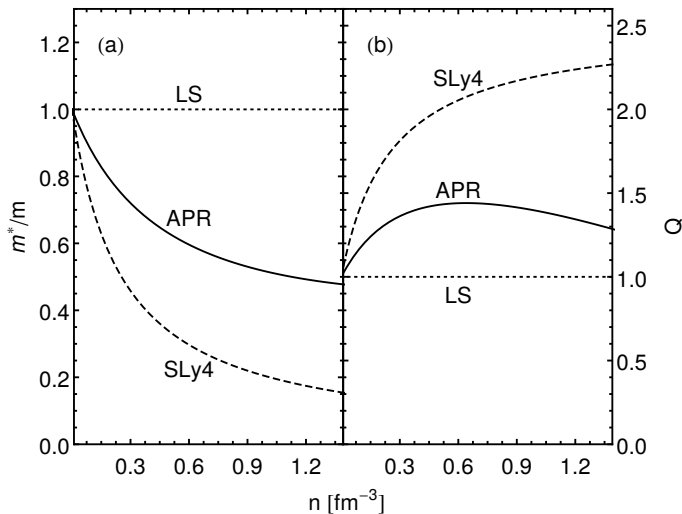


FIG. 2. The effective mass ratio m^*/m and the quantity $Q = 1 - (3n/2m^*)dn/dm^*$ vs density in PNM for the APR, LS and SLy4 models.

β_f	0.5	0.7	0.9	Not Fixed
Prop.				
n_f (fm^{-3})	0.515	0.705	0.951	N/A
M_{max} (M_\odot)	2.23	2.29	2.30	2.30
R_{max} (km)	12.03	11.70	11.58	11.58
n_c (fm^{-3})	0.875	0.906	0.915	0.915
ϵ_c (MeV fm^{-3})	1101.6	1175.9	1197.7	1197.7
P_c (MeV fm^{-3})	398.0	534.0	584.1	584.1

TABLE III. Same as Table II, but for the LS model.

ture (right panel) for a fixed $\beta_f = 0.9$. That the different curves appear to be causally fixed at the same density is a consequence of the (accidental) fact that, for APR, $n_f(\beta_f = 0.9) \simeq n_X$. As a caution we point out that the problematic implementation of [6] will appear correct if one chooses $\beta_f = \beta_f(n_X)$.

β_f	0.5	0.7	0.9	Not Fixed
Prop.				
n_f (fm^{-3})	0.634	0.825	1.048	N/A
M_{max} (M_\odot)	1.95	2.03	2.05	2.05
R_{max} (km)	10.46	10.20	10.03	10.00
n_c (fm^{-3})	1.150	1.173	1.195	1.196
ϵ_c (MeV fm^{-3})	1454.2	1534.4	1590.7	1594.0
P_c (MeV fm^{-3})	530.0	717.1	852.6	872.1

TABLE IV. Same as Table II, but for the SLy4 model.

A notable feature of the results in Fig. 3 is that $(c_s/c)^2 = 0.9$ for all $n \geq n_a$, the density at which acausality sets in for the APR model. With a density-dependent β_f , a gradual approach of $(c_s/c)^2$ to 1 may be achieved. Figure 4 shows results with the density-dependent β_f given by Eq. (51). As noted earlier, many other possibilities also exist as long as one can find a tractable, preferably analytical, solution to Eq. (33).

The implementation of causality introduces modifications to the total energy density ϵ , pressure P , chemical potential μ , the specific heats C_V and C_P , and the adiabatic index Γ_S which are exhibited in Figs. 5-10, respectively. All of these results correspond to $\beta_f = 0.9$. These modifications occur at high densities and are more pronounced for quantities (P , μ , Γ_S and C_P) that involve density derivatives of the energy. This observation is in accordance with that made earlier regarding the central pressure of neutron stars. Results corresponding to Eq. (51) are nearly identical and are not shown here.

Comparison with finite-range force models

Here we contrast the above results for $(c_s/c)^2$ with those of a nonrelativistic potential model with finite-range forces at finite temperature studied in detail in Ref. [5], where results for $(c_s/c)^2$ were, however, not shown.

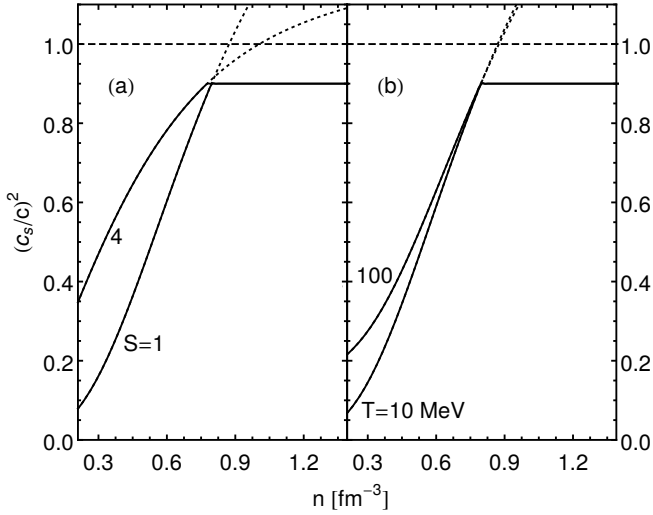


FIG. 3. Squared speed of sound in PNM for the APR model with (solid curves) and without (dotted curves) causality enforced with $\beta_F = 0.9$ for fixed entropy (a) and temperature (b) vs density.

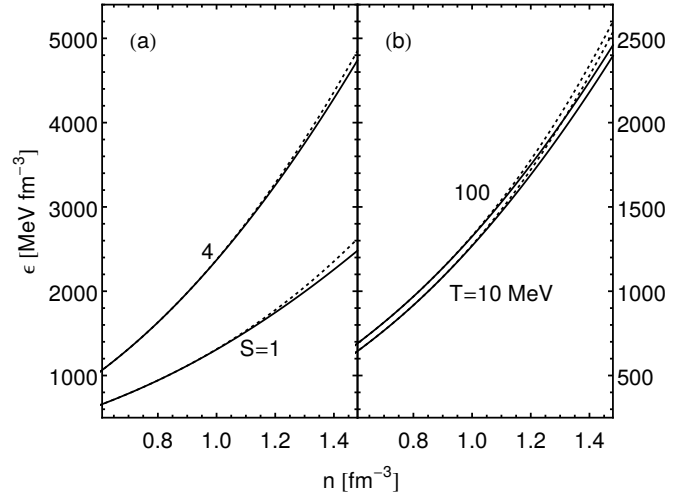


FIG. 5. Total energy density of PNM for the APR model with (solid curves) and without (dotted curves) causality enforced with $\beta_f = 0.9$ for fixed entropy (a) and temperature (b) vs density.

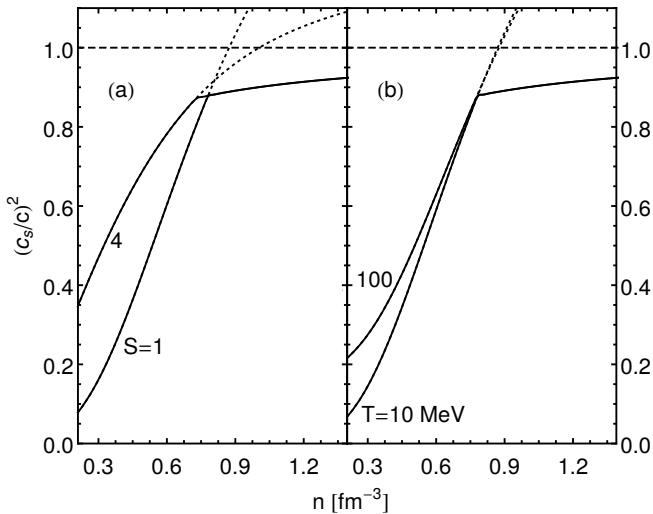


FIG. 4. Same as Fig. 3, but with the density-dependent β_f given by Eq. (51).

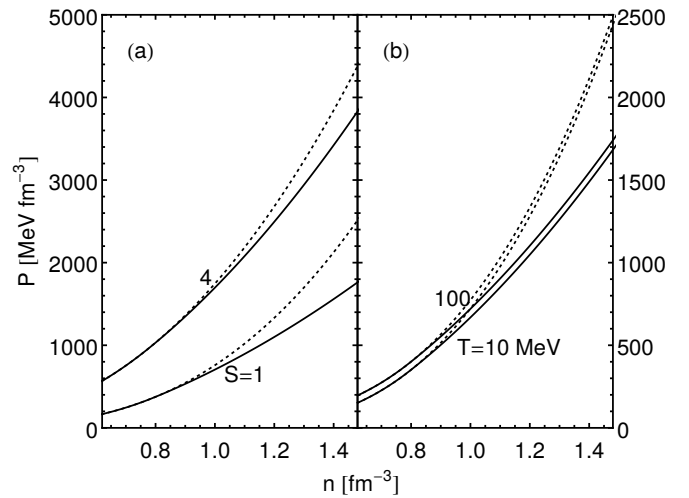


FIG. 6. Pressure of PNM for the APR model with (solid curves) and without (dotted curves) causality enforced with $\beta_f = 0.9$ for fixed entropy (a) and temperature (b) vs density.

For PNM, the energy density in this model is

$$\epsilon = 2 \int \frac{d^3k}{(2\pi)^3} \frac{\hbar^2 k^2}{2m} f + Au^2 + \frac{Bu^\sigma}{1 + B'u^{\sigma-1}} + u \sum_{i=1,2} C_i 2 \int \frac{d^3k}{(2\pi)^3} \frac{1}{[1 + (k/\Lambda_i)^2]} f, \quad (77)$$

where $u = n/n_s$, f is the usual Fermi-Dirac distribution function at finite T , and the parameters A , B , σ , C_i , B' , and Λ_i are determined from constraints provided by the empirical properties of nuclear matter at

n_s . Referred to as BPAL33 in Ref. [5], their numerical values are: $A = 1.627$, $B = 8.908$, $B' = 0.422$, $C_1 = -106.7$ MeV, $C_2 = 6.544$ MeV, $\Lambda_1 = 1.5\hbar k_F^{(0)}$, and $\Lambda_2 = 3.0\hbar k_F^{(0)}$ with $k_F^{(0)} = (3\pi^2 n_s/2)^{1/3}$. Note the redefinition of parameters here from those in the original reference. The energy density in Eq. (77) differs from that of zero-range Skyrme-like models including the APR model in two respects. First, the term encapsulating the influence of higher-than two body forces is such that it does not lead to an acausal behavior at $T = 0$. Secondly, the

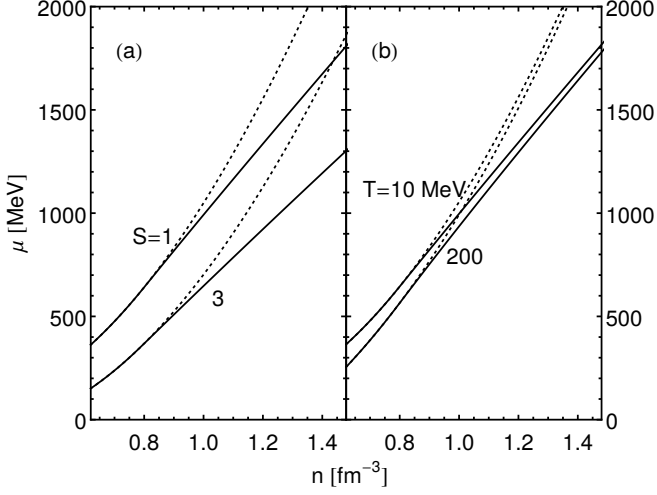


FIG. 7. Chemical potential in PNM for the APR model with (solid curves) and without (dotted curves) causality enforced with $\beta_f = 0.9$ for fixed entropy (a) and temperature (b) vs density.

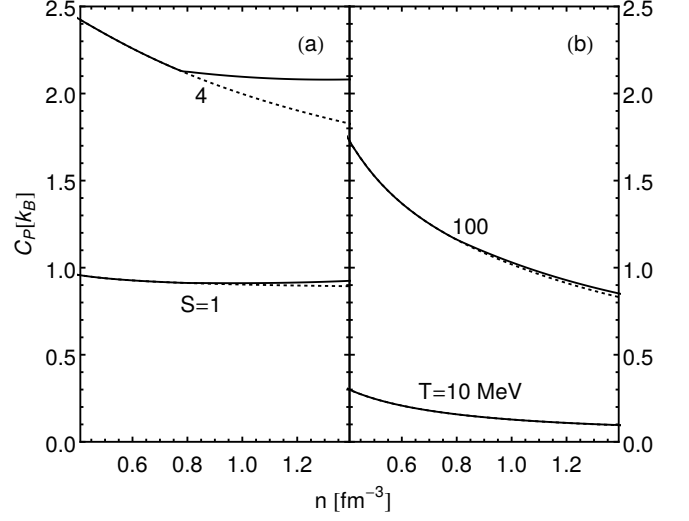


FIG. 9. Specific heat at constant pressure in PNM for the APR model with (solid curves) and without (dotted curves) causality enforced with $\beta_f = 0.9$ for fixed entropy (a) and temperature (b) vs density.

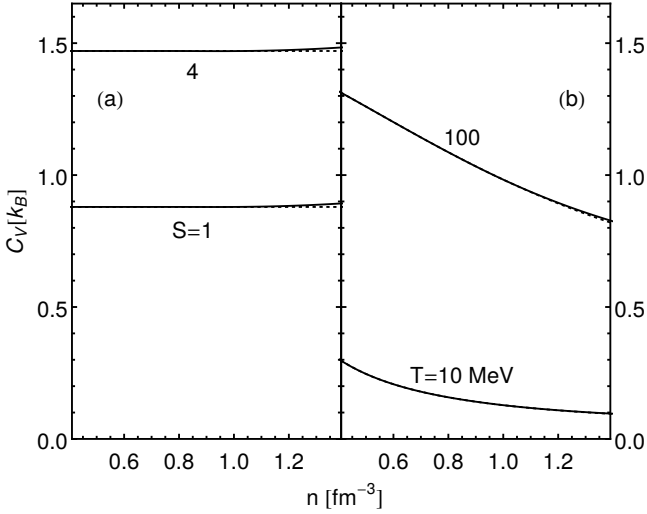


FIG. 8. Specific heat at constant volume in PNM for the APR model with (solid curves) and without (dotted curves) causality enforced with $\beta_f = 0.9$ for fixed entropy (a) and temperature (b) vs density.

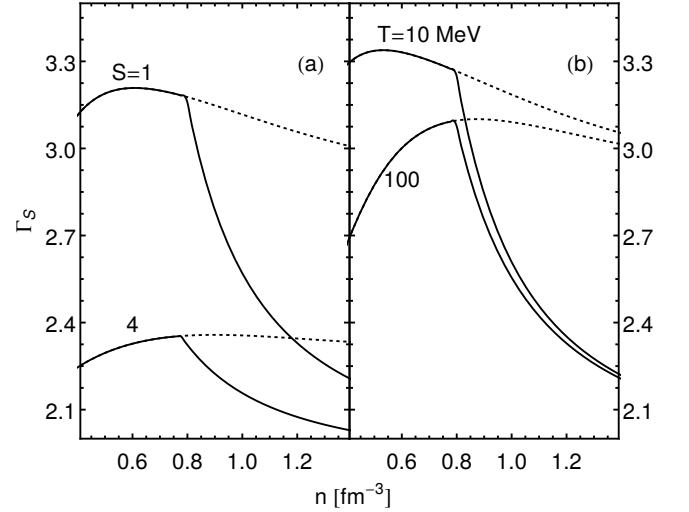


FIG. 10. Adiabatic index in PNM for the APR model with (solid curves) and without (dotted curves) causality enforced with $\beta_f = 0.9$ for fixed entropy (a) and temperature (b) vs density.

finite-range terms lead to an effective mass

$$\frac{m^*}{m} = \left[1 + \sum_{i=1,2} \alpha_i u \left(1 + \frac{(2u)^{2/3}}{R_i^2} \right) \right]^{-1}, \quad (78)$$

where $R_i = \Lambda_i / (\hbar k_F^{(0)})$, that saturates for $n \gg n_s$ as shown in Fig. 11. As a result, $Q < 1.2$ and $dQ/dn < 0$ for $n > n_s$ which implies that $c_s < c$ in the limit $T \rightarrow \infty$ [Eq. (21)]. This means that $c_s < c$ for all T being that the

possible paths that c_s can traverse in (n, T) are bounded by $c_s(T = 0)$ and $c_s(T \rightarrow \infty)$. In closing this section we note that, for BPAL33, the intersection density $n_X = 0.853 \text{ fm}^{-3}$.

To preserve causality, two lessons, of much value to first principle microscopic calculations hot and dense matter, are learned from the results above. First, contributions from higher than two-body forces must be screened at high density at the $T = 0$ level. Secondly,

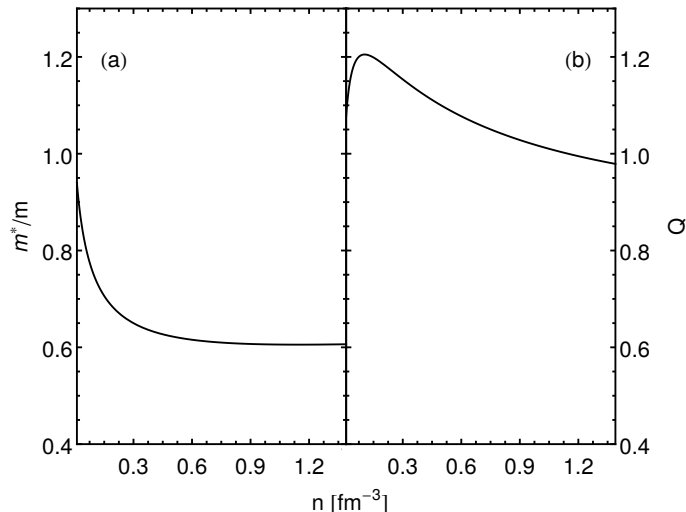


FIG. 11. The effective mass ratio m^*/m and the quantity $Q = 1 - (3n/2m^*)dn/dm^*$ vs density in PNM for the BPAL33 model.

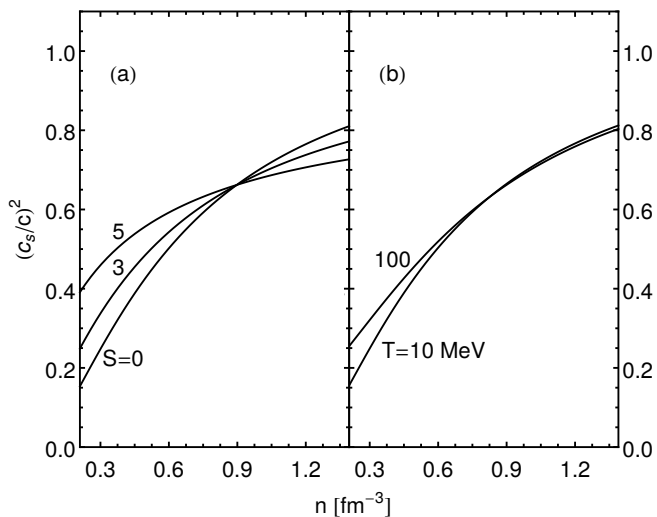


FIG. 12. Squared speed of sound in PNM for the BPAL33 model for fixed entropy (a) and temperature (b) vs density.

the nucleon effective mass, which controls thermal effects, must not rapidly decrease with density as in some Skyrme-like models that employ only contact interactions. The use of finite-range forces (as in first principle calculations of dense matter), which tends to saturate the nucleon effective mass, mitigates the influence of thermal effects in making EOS's acausal.

VI. SUMMARY AND CONCLUSIONS

In this work, we have proposed a method by which non-relativistic EOS's that become acausal at high densities

can be modified so that they remain causal at all densities and entropies/temperatures. This approach is easily implemented and computationally straightforward; its most important feature is thermodynamic consistency. Illustrative calculations are presented both for a fixed value of the speed of sound c_s in the “causality-enforcement” region as well as for continuous functions of density and entropy per baryon (n, S) which approach c asymptotically from below.

As examples, we have explored consequences of enforcing causality to the attributes of maximum-mass neutron star configurations in pure neutron matter for the APR, LS, and SLy4 models. The EOS functions of the APR model are presented for entropies per baryon of relevance to astrophysical simulations before and after enforcing causality. Our principal findings are summarized below.

Insofar as our choice for the “new” speed of sound c_s is close to c , we find that both cold and finite- T properties associated with the energy density, ε , and the specific heat at constant volume, C_V , are relatively weakly affected after enforcing causality. However, properties such as the pressure, P , the chemical potential, μ , and the specific heat at constant pressure, C_P , which are related to density derivatives of the energy exhibit larger variations compared to ε and C_V . At $T = 0$, the basic characteristics of PNM-NS configurations such as their central density, n_c , the maximum mass, M_{max} , and the radius of the maximum configuration, R_{max} , are not greatly affected by enforcing causality. However, for models (such as SLy4) in which the effective nucleon mass drops rapidly with density thermal effects cause c_s to exceed c at densities significantly lower than at $T = 0$. An interesting finding is that in the extreme nondegenerate limit, c_s for models with contact interactions such as those considered here decouples from entropy/temperature and is instead determined by the Landau effective mass and its derivatives with respect to density.

Finally, our study of a schematic potential model illustrates that in first principle calculations of hot and dense matter, contributions from higher than two-body interactions must be screened and effective masses determined by finite-range forces must saturate at high density to preserve causality.

ACKNOWLEDGMENTS

Research support for M.P. by the U.S. DOE under Grant No. DE-FG02-93ER-40756 is gratefully acknowledged.

-
- [1] P. Demorest, T. Pennucci, S. Ransom, M. Roberts, and J. Hessels, *Nature* **467**, 1081 (2010).
- [2] J. Antoniadis, P. C. C. Freire, N. Wex, and *et al.*, *Science* **340** (2013).
- [3] B. P. Abbott and *et al.*, *Phys. Rev. Lett.* **116**, 061102 (2016).
- [4] B. P. Abbott and *et al.*, *Phys. Rev. Lett.* **116**, 241103 (2016).
- [5] M. Prakash *et al.*, *Phys. Rep.* **280**, 1 (1997).
- [6] C. Constantinou, B. Muccioli, M. Prakash, and J. M. Lattimer, *Phys. Rev. C* **89**, 065802 (2014).
- [7] S. A. Bludman and C. Dover, *Phys. Rev. D* **22**, 1333 (1980).
- [8] M. Prakash, T. L. Ainsworth, and J. M. Lattimer, *Phys. Rev. Lett* **61**, 2518 (1988).
- [9] P. Armani *et al.*, *J. Phys. Conf. Ser.* **336**, 012014 (2011).
- [10] S. Gandolfi, J. Carlson, and S. Reddy, *Phys. Rev. C* **85**, 032801 (2012).
- [11] G. Wlazlowski, J. W. Holt, S. Moroz, A. Bulgac, and K. J. Roche, *Phys. Rev. Lett.* **113**, 182503 (2014).
- [12] A. Gezerlis and J. Carlson, *Phys. Rev. C* **81**, 025803 (2010).
- [13] K. Hebeler and A. Schwenk, *Phys. Rev. C* **82**, 014314 (2010).
- [14] L. Coraggio, J. W. Holt, N. Itaco, R. Machleidt, and F. Sammarruca, *Phys. Rev. C* **87**, 014322 (2013).
- [15] I. Tews, T. Krüger, K. Hebeler, and A. Schwenk, *Phys. Rev. Lett.* **110**, 032504 (2013).
- [16] H. Togashi and M. Takano, *Nucl. Phys. A* **902**, 53 (2013).
- [17] J. E. Lynn *et al.*, *Phys. Rev. Lett.* **116**, 062501 (2016).
- [18] E. Epelbaum, H. Krebs, D. Lee, and U.-G. Meissner, *Eur. Phys. J. A* **40**, 199 (2009).
- [19] J. Hu, Y. Zhang, E. Epelbaum, U.-G. Meissner, and J. Meng, arXiv:1612.05433v1.
- [20] M. Nauenberg and G. Chapline, *Astrophys. J.* **179**, 277 (1973).
- [21] J. M. Lattimer, M. Prakash, D. Masak, and A. Yahil, *Astrophys. J.* **355**, 241 (1990).
- [22] J. M. Lattimer and F. D. Swesty, *Nucl. Phys.* **A535**, 331 (1991).
- [23] E. Chabanat, P. Bonche, P. Haensel, J. Meyer, and R. Schaeffer, *Nucl. Phys.* **A635**, 231 (1998).
- [24] A. Akmal, V. R. Pandharipande, and D. G. Ravenhall, *Phys. Rev. C* **58**, 1804 (1998).
- [25] L. Landau and E. M. Lifshitz, *Fluid Mechanics, Volume 6, 2nd Edition* (Butterworth-Heinemann, Oxford, 1987).
- [26] S. Weinberg, *Astrophys. J.* **168**, 175 (1971).
- [27] J. Guichelaar, *Physica (Amsterdam)* **74**, 330 (1974).
- [28] M. Prakash, in *Nuclear Equation of State*, edited by A. Ansari and L. Satpathy, p. 229, Singapore, 1996, World Scientific.
- [29] C. Constantinou, B. Muccioli, M. Prakash, and J. M. Lattimer, *Phys. Rev. C* **92**, 025801 (2015).
- [30] G. Baym and C. Pethick, *Landau Fermi-Liquid Theory* (Wiley Interscience, New York, 1991).
- [31] M. Prakash, T. L. Ainsworth, J. P. Blaizot, and H. Wolter, in *Windsurfing the Fermi Sea, Volume II*, edited by T. T. S. Kuo and J. Speth, p. 357, Amsterdam, 1987, Elsevier.
- [32] S. M. Johns, P. J. Ellis, and J. M. Lattimer, *Astrophys. J.* **473**, 1020 (1996).